

Airy minima in the scattering of weakly bound light heavy ions

F. Michel

Université de Mons-Hainaut, Place du Parc, 20, B-7000 Mons, Belgium

S. Ohkubo

Department of Applied Science and Environment, Kochi Women's University, Kochi 780-8515, Japan

(Received 22 November 2004; published 9 November 2005)

We reanalyze the existing ${}^6\text{Li} + {}^{12}\text{C}$ elastic scattering angular distributions for incident energies ranging from a few MeV to 318 MeV within the frame of the optical model. Despite the important breakup effects expected in the scattering of such a fragile projectile, the system is found to display a surprising transparency. Indeed the barrier-wave/internal-wave decomposition of the elastic scattering amplitude reveals that a substantial part of the incident flux that penetrates the nuclear interior reemerges in the elastic channel, and typical refractive effects, like Airy minima, are clearly identified in the angular distributions. Coupled channel calculations performed on ${}^{12}\text{C}({}^6\text{Li}, {}^6\text{Li}'){}^{12}\text{C}^*(J^\pi = 2^+, E_x = 4.44 \text{ MeV})$ angular distributions extending through the whole angular range confirm the existence of an important internal-wave contribution in the backward hemisphere. A similar transparency is observed in other systems of this mass region, such as ${}^7\text{Li} + {}^{12}\text{C}$ or ${}^6\text{Li} + {}^{16}\text{O}$. Finally, we examine recent ${}^6\text{He} + {}^{12}\text{C}$ elastic scattering data obtained at 18 MeV by Milin *et al.* [Nucl. Phys. **A730**, 285 (2004)] and extending up to $\theta_{\text{c.m.}} \simeq 85^\circ$, and we suggest additional measurements that could ascertain whether some transparency persists in the scattering of this radioactive projectile.

DOI: [10.1103/PhysRevC.72.054601](https://doi.org/10.1103/PhysRevC.72.054601)

PACS number(s): 24.10.Ht, 25.60.Bx, 25.70.Bc

I. INTRODUCTION

Impressive advances in the field of radioactive nuclear beams (RNB) have made possible precise and reliable measurements of elastic, inelastic, and transfer cross sections of loosely bound projectiles such as ${}^6\text{He}$. The ${}^{12}\text{C}({}^6\text{He}, {}^6\text{He})$ elastic angular distribution has recently been measured at 18 MeV for c.m. angles extending up to 85° [1]; in this angular range, the experimental angular distribution is very similar to that obtained for the neighboring ${}^{12}\text{C}({}^6\text{Li}, {}^6\text{Li})$ system at comparable incident energies.

For systems involving fragile projectiles such as ${}^6\text{He}$ (and, to a lesser extent, ${}^6\text{Li}$), breakup effects are expected to play an important role in the scattering mechanism; in fact, a strong reduction of the real part of the folding model potential has been found necessary to describe the ${}^6\text{Li}$ experimental data [2–4], whereas more strongly bound projectiles such as ${}^4\text{He}$ do not require such a renormalization. Breakup is also expected to be responsible for a strong enhancement of the imaginary part of the optical potential. The influence of breakup effects on ${}^6\text{Li}$ scattering has been intensively investigated by several authors [5–7].

Strong absorption effects usually dominate the scattering of many light and heavy ions, making the scattering angular distributions only sensitive to the far tail of the interaction potential. However, several systems—such as $\alpha + {}^{16}\text{O}$ and $\alpha + {}^{40}\text{Ca}$ [8], or ${}^{16}\text{O} + {}^{16}\text{O}$ and ${}^{16}\text{O} + {}^{12}\text{C}$ [9–13]—display enough transparency to make the scattering sensitive to the interaction at distances smaller than that of the nuclear surface. At low energy, this transparency manifests itself by the now classical anomalous large angle scattering (ALAS) phenomenon [8], which consists in a spectacular enhancement of the cross section at back angles, accompanied by strongly energy-dependent interference phenomena [8, 10, 12]; at higher

energy, the angular distribution turns into a distinctive rainbow pattern [8, 11, 13], preceded at intermediate angles by one or several broad oscillations, which have been interpreted in terms of an Airy mechanism [9–19].

In the case of the much studied ${}^6\text{Li} + {}^{12}\text{C}$ system, such a behavior, indicative of an incomplete absorption, has paradoxically been observed for a long time but seems to have remained largely unnoticed; indeed the low-energy data display a strong ALAS behavior, clearly seen, for example, in the old 30.6-MeV data of Chuev *et al.* [20], which extend over the whole angular range. The same phenomenon is observed at 29.8 MeV in the neighboring ${}^6\text{Li} + {}^{16}\text{O}$ system [20], for which the data also extend up to large angles. Still, at that time, the significance of this backward rise was overlooked, and the analysis of Bassani *et al.* [21] concludes that “ ${}^6\text{Li}$ behaves as a strongly absorbed projectile.” These data are well described within the optical model (OM), if use is made of a moderate absorption; and a semiclassical decomposition of the elastic scattering amplitude into its so-called barrier-wave and internal-wave (B/I) contributions [22] confirmed later, in an unambiguous way [23], that the ${}^6\text{Li} + {}^{16}\text{O}$ system displays a surprising transparency: Indeed, the backward enhancement is completely dominated by that part of the incident flux that crosses the potential barrier and reemerges in the elastic channel after penetrating the nuclear interior. In fact the transparency of the system is so high that in the 29.8-MeV ${}^{16}\text{O}({}^6\text{Li}, {}^6\text{Li})$ angular distribution the influence of the internal-wave component can be felt at angles as small as 50° !

Investigation of the existing ${}^{12}\text{C}({}^6\text{Li}, {}^6\text{Li})$ data confirms the transparency of the system up to high incident energies; in particular rainbow scattering is observed above about 60 MeV, with the occurrence of a well-marked Airy minimum (A1). This transparency has recently been rediscovered by Carstou *et al.* [24], who identified what they call an “exotic feature”

in the data around 50 MeV, consisting of the appearance of a broad plateau at intermediate angles [25]. This plateau is in fact the small-angle side of a broad dip, which is nothing but the A1 Airy minimum at that energy; this minimum progressively moves to smaller angles as energy increases.

The purpose of this paper is to reanalyze in a systematic way the existing ${}^6\text{Li} + {}^{12}\text{C}$ elastic scattering data for incident energies ranging from a few MeV to 318 MeV, having in mind the investigation of the surprising transparency displayed by this system; the semiclassical techniques of the nearside/farside (N/F) and B/I decompositions [22,26] will be heavily relied upon for this purpose. An important point of the study will be to identify the various Airy minima that appear in the angular distributions as energy increases—a crucial ingredient in the unambiguous determination of the interaction potential. Finally, the new ${}^6\text{He} + {}^{12}\text{C}$ data will be revisited in the light of the results obtained for its companion system.

The paper is organized as follows. In Sec. II, we subject the whole available set of ${}^6\text{Li} + {}^{12}\text{C}$ experimental elastic scattering data to a global OM analysis. Although several phenomenological global analyses of the data have been proposed in the literature [25,27–29], it is worth repeating them since some encounter serious difficulties in reproducing the data at large angles, whereas others report discontinuities in the energy dependence of the parameters or the need to include additional phenomenological devices such as a J -dependent absorption. In Sec. III, the energy dependence of the elastic scattering angular distributions is investigated, with an emphasis on the identification of the Airy minima for this system; the few available ${}^{12}\text{C}({}^6\text{Li}, {}^6\text{Li}'){}^{12}\text{C}^*(J^\pi = 2^+, E_x = 4.44 \text{ MeV})$ angular distributions extending over the whole angular range are also investigated within the frame of coupled channel calculations and subjected to a B/I analysis. Section IV is devoted to a brief discussion of the refractive effects observed in the neighboring ${}^6\text{Li} + {}^{16}\text{O}$ and ${}^7\text{Li} + {}^{12}\text{C}$ systems. Finally, we analyze in Sec. V the newly available ${}^6\text{He} + {}^{12}\text{C}$ elastic scattering data [1], and we suggest additional measurements that could provide decisive arguments in favor of a possible transparency for that system; a summary and our conclusions can be found in Sec. VI.

II. OPTICAL MODEL ANALYSIS

Many ${}^6\text{Li} + {}^{12}\text{C}$ elastic scattering angular distributions are available for incident energies between a few MeV and 318 MeV [20,24,25,27–35], some of them extending over the whole angular range; these data have been analyzed by several groups within the frame of the optical model, either in a purely phenomenological way and/or within the frame of the folding model using various nucleon-nucleon effective interactions [6,21,24,25,27–37]. In the latter case, it has generally been found that, contrary to what is observed for more strongly bound light ions, the real part of the folding model potential has to be reduced by multiplying it by a factor N_R equal to about 0.6, an effect attributed to the breakup of the soft ${}^6\text{Li}$ projectile whose separation energy into $\alpha + \text{deuteron}$ does not exceed 1.5 MeV. A closer

investigation of the breakup mechanism indicates that the associated dynamical polarization potential (DPP) cannot be represented by a simple renormalization of the bare potential, and indeed the very detailed folding model investigation of Khoa *et al.* [37] between 60 and 318 MeV, using one of the best density-dependent nucleon-nucleon effective interactions, locates in the surface region the (repulsive) spline correction that has to be added to the real part of the folding potential to describe quantitatively the data.

Most of the existing folding model analyses have been restricted to medium to high energies, and the analyses of the low-energy data—or the global analyses including low-energy data—have generally been carried out in a phenomenological framework, using conventional form factors of the Woods-Saxon type. The global analyses [25,27–29] have often suffered from several defects, such as a poor reproduction of the large-angle data at low energy, or the need for introducing a discontinuity in the shape of the potential used as energy increases; the effect of, for example, a spin-orbit interaction [25,27] or of a J dependence of the imaginary part of the potential [25] have sometimes been invoked or introduced in the analysis.

It has repeatedly been pointed out [8] that the usual Woods-Saxon form factor does not approximate the shape of the folding model potential in a satisfactory way and that alternative form factors like the Woods-Saxon squared potential are better suited for that purpose. Before embarking in more complicated calculations, we therefore investigated the possibility of reproducing the existing data within the OM, using a Woods-Saxon squared form factor for the real part of the potential; our aim is to obtain a good quality, global description of the data, embodying all the salient features of experiment. After performing individual fits at selected energies, it proved possible to obtain an adequate representation of the data using a real potential with a Woods-Saxon squared shape having a fixed geometry; the imaginary part of the potential is also of Woods-Saxon squared shape, and we use a Coulomb potential of the point-sphere type with a radius $R_c = 1.3(6^{1/3} + 12^{1/3}) = 5.3 \text{ fm}$. The optical potential used thus reads

$$U(r) = V(r) + iW(r) \\ = V_c(r) - V_0 f(r; R_R, a_R) - iW_0 f(r; R_I, a_I), \quad (1)$$

where

$$f(r; R, a) = \frac{1}{\{1 + \exp[(r - R)/2a]\}^2}. \quad (2)$$

The radius and the diffuseness of the real part of the potential are fixed to the values $R_R = 3.20 \text{ fm}$ and $a_R = 0.7 \text{ fm}$; the remaining parameters, that is, the depth V_0 of the real part of the potential and the three imaginary potential parameters, were adjusted independently at each of the energies where an angular distribution covering most of the angular range—or extending well beyond the rainbow angle at high energy—was available, that is, at 13 [28], 24 and 30 [29], 59.8 [30], 99 [31], 124 [32], 156 [33], 168.6 [32], 210 [34], and 318 MeV [35]. The results obtained are plotted in Fig. 1, and the extracted parameters are displayed in Table I, where we also

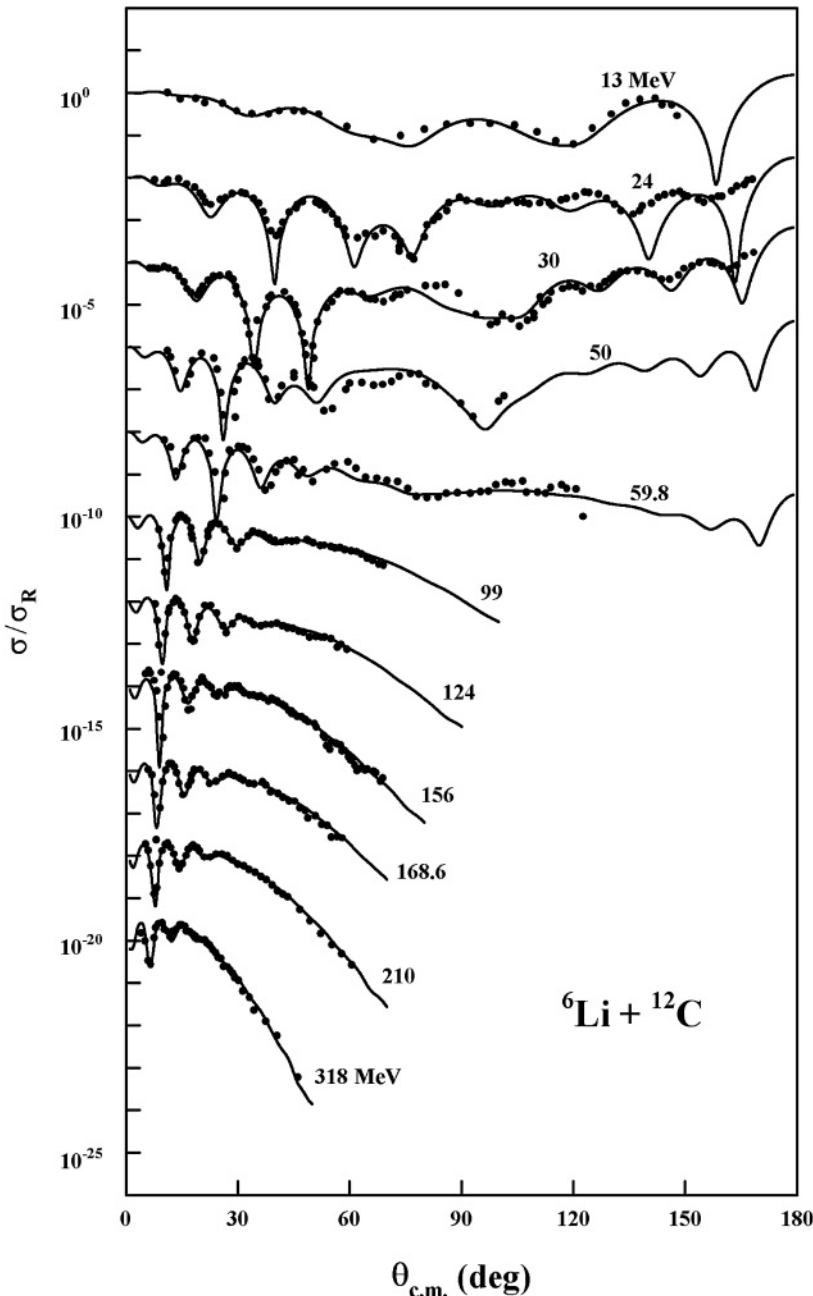


FIG. 1. Global optical model description of the experimental ${}^6\text{Li} + {}^{12}\text{C}$ elastic scattering angular distributions for incident energies between 13 and 318 MeV [25,27–35]. (The 13-MeV curve is normalized correctly, and each successive curve is displaced by a factor of 100 with respect to the previous one.)

give the volume integrals per pair of nucleons $j_V = J_V/72$ and $j_W = J_W/72$ of the real and imaginary parts of the potential; these quantities are known to be generally better determined than the individual parameters of the potential and will be useful for comparison with earlier work. As there is a large gap in energy in the available complete angular distributions between 30 and 60 MeV, Fig. 1 and Table I also include the incomplete 50-MeV angular distribution [25]; at that energy the geometry of the imaginary potential was fixed somewhat arbitrarily by comparison with the neighboring energies to the values $R_I = 5$ fm and $a_I = 0.85$ fm, and the real and imaginary well depths were the only parameters to be adjusted to experiment.

Although the agreement with experiment is not always perfect, Fig. 1 shows that the main trends of the data

are satisfactorily reproduced by this very simple potential. At low energy (especially at 24 MeV) the disagreement with the phasing of the data at large angles could be due to intermediate structure effects, which for example persist in the $\alpha + {}^{16}\text{O}$ case up to about 30 MeV [38,39]. And at higher energy (30–60 MeV) the DPP associated with ${}^6\text{Li}$ breakup cannot possibly be incorporated satisfactorily within the simple form factor used here [37]. Still the model describes well the energy dependence of the position of the broad minima seen in the data up to 60 MeV incident energy. A look at Table I indicates a smooth evolution with energy of the real and imaginary parts of the potential; the most significant quantities, that is, their volume integrals per nucleon pair j_V and j_W , are plotted in Fig. 2 as a function of the c.m. energy of the system. These volume integrals are in reasonable agreement with those of the

TABLE I. Parameters of the global optical potential (with $R_R = 3.20$ fm, $a_R = 0.70$ fm and $R_c = 5.3$ fm) describing the experimental $^{12}\text{C}(^6\text{Li}, ^6\text{Li})$ elastic scattering data between 13 and 318 MeV [25,28–35], together with the volume integrals per nucleon pair j_V and j_W of the real and imaginary parts of these potentials. (Energies are in MeV, lengths in fm, and volume integrals in MeV fm^3 .)

E_{lab}	V_0	W_0	R_I	a_I	j_V	j_W
13	248.5	4.72	6.23	0.35	402.9	51.4
24	245.7	11.4	5.03	0.49	398.3	60.6
30	235.1	14.7	4.65	0.94	381.1	70.0
50.0	220.0	17.0	5.00	0.85	356.7	93.7
59.8	211.4	44.0	4.05	0.84	342.7	140.7
99	178.1	47.2	4.03	0.77	288.6	142.5
124	178.0	48.6	4.10	0.79	288.5	155.3
156	172.7	65.3	3.75	0.69	280.0	156.2
168.6	174.5	65.1	3.60	0.85	282.9	157.9
210	175.6	90.0	3.27	0.81	284.7	169.4
318	167.9	70.3	3.85	0.68	272.2	178.7

folding + spline analysis of Khoa *et al.* [37] and of the double folding model analysis of Carstoiu *et al.* [24].

It is relevant to compare these volume integrals with those obtained for the $\alpha + ^{16}\text{O}$ system, which involves a light, strongly bound projectile and for which breakup effects are negligible; the values obtained for that system are also plotted in Fig. 2 as a function of the c.m. energy, using the global potential of Ref. [39], which describes quantitatively the data between 32 and 146 MeV. For the $\alpha + ^{16}\text{O}$ system, the real

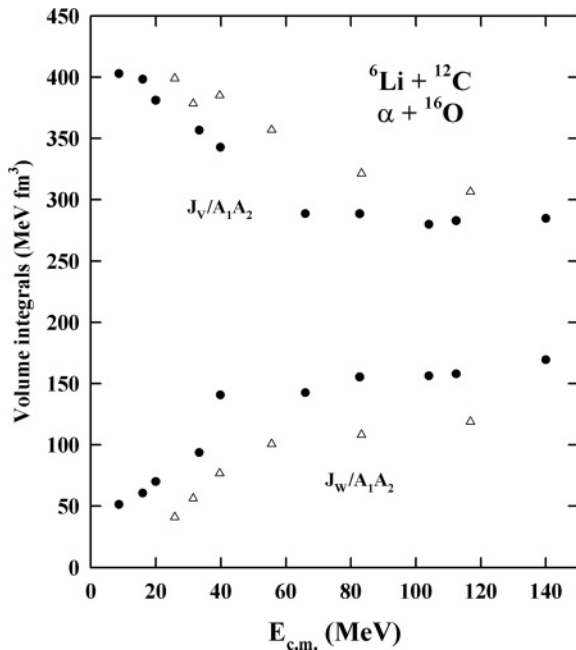


FIG. 2. Energy dependence of the volume integrals per pair of nucleons of the real and imaginary parts of the $^6\text{Li} + ^{12}\text{C}$ global optical potential of the present work (dots), as compared with that obtained for the $\alpha + ^{16}\text{O}$ system at comparable c.m. energies [39] (triangles).

volume integral behavior is adequately represented by the following linear prescription [39]:

$$J_V/64 = 418.1(1 - 0.00196E_\alpha) \text{ MeV fm}^3. \quad (3)$$

At low and high energy, the real volume integrals are seen to take comparable values for both systems, but at intermediate energy the $^6\text{Li} + ^{12}\text{C}$ volume integral is substantially smaller than its $\alpha + ^{16}\text{O}$ counterpart. The difference is maximum around $E_{\text{c.m.}} \simeq 70$ MeV ($E_{\text{lab}} \simeq 100$ MeV), that is, at an incident energy where the DPP associated with ^6Li breakup is found to be maximum [37]. However, the imaginary volume integral is substantially larger in the ^6Li case, but as will be seen in Sec. III absorption remains nonetheless incomplete, and strong refractive effects, which dominate $\alpha + ^{16}\text{O}$ scattering at low and intermediate energy, do indeed survive in the $^6\text{Li} + ^{12}\text{C}$ system.

III. INVESTIGATION OF REFRACTIVE EFFECTS IN $^{12}\text{C}(^6\text{Li}, ^6\text{Li})$ SCATTERING

At low energy the $\alpha + ^{16}\text{O}$ elastic scattering angular distributions display a vigorous ALAS behavior, which tends to subside as energy increases: Beyond about 50 MeV incident energy the backward enhancement is progressively replaced by the exponential decrease characteristic of rainbow scattering at large angles [39]. A comparison of Fig. 1 of the present paper with Fig. 1 in Ref. [39] reveals striking similarities between the $^6\text{Li} + ^{12}\text{C}$ and the $\alpha + ^{16}\text{O}$ systems; in particular broad minima, shifting progressively to smaller angles as energy increases, are apparent in both sets.

Semiclassical approaches have successfully been invoked to interpret this type of complicated scattering patterns. In the most popular one, the so-called nearside/farside approach [26], the elastic scattering amplitude is split into two contributions corresponding to classical trajectories with a positive/negative deflection angle; this decomposition can be incorporated easily in any OM code [26]. In this picture, the broad minima seen in the angular distributions are carried by the farside component of the amplitude; this is, for example, the case for $^6\text{Li} + ^{12}\text{C}$ at 30 MeV incident energy [Fig. 3(a)] where a broad minimum is observed around 100° . The presence of minima in the farside contribution to the scattering amplitude can only be explained in terms of an interference (negative-angle) trajectories with different impact parameters [9,14–19]. The presence of these minima in the farside component is by itself an indication of a particular transparency of the system, since an increase of absorption washes out the interference structure; these minima are often called Airy minima [9,16–19], although recent studies indicate that their origin is different from that of their meteorological counterpart [40]. The minimum around 100° must in fact be labeled A2, since as will be shown below an additional broad minimum appears at large angles at higher energy, just before the onset of rainbow scattering. Another minimum is also observed in the farside contribution at 30 MeV around 50° (and in the full angular distribution as a depression in the diffractive oscillations) and must thus be labeled A3.

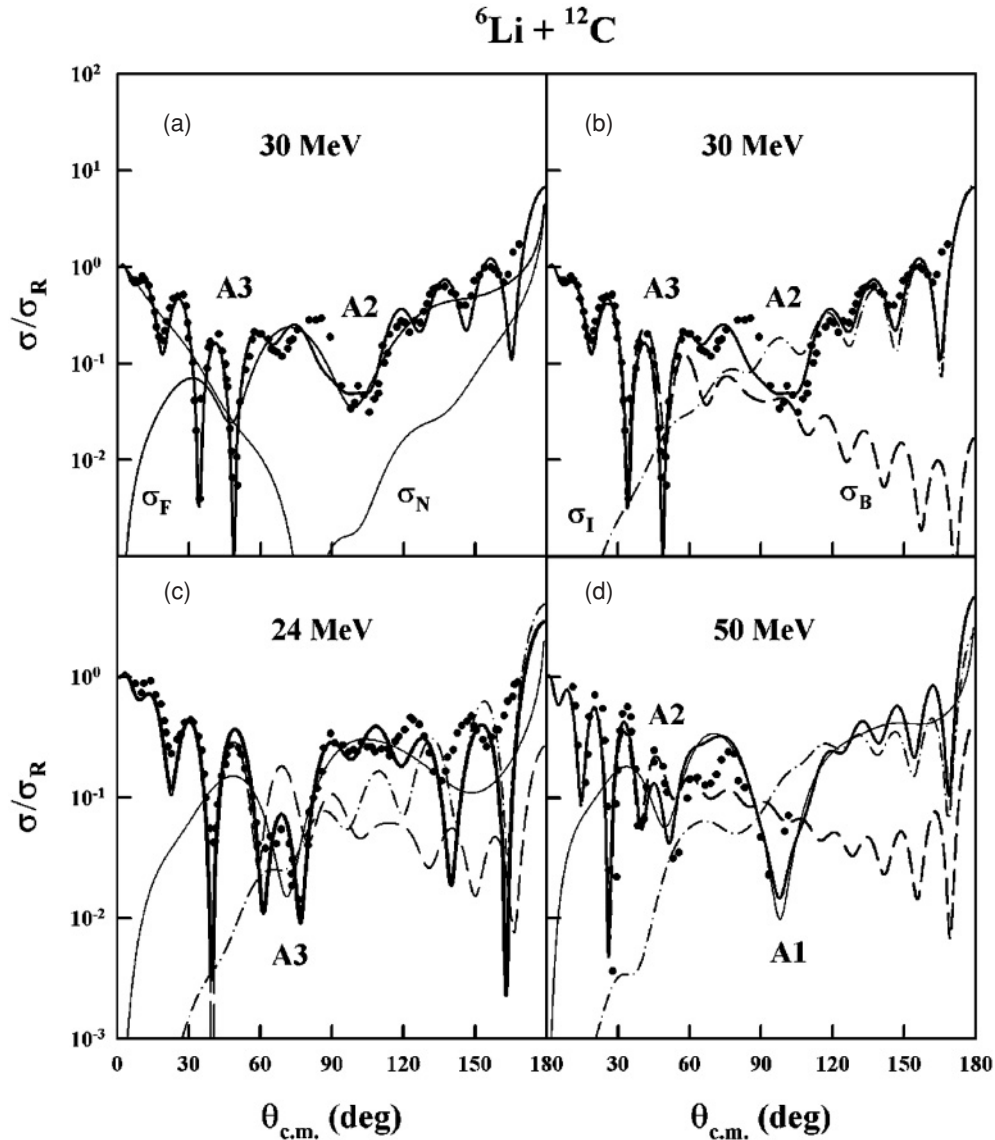


FIG. 3. Optical model and experimental [25,29] elastic ${}^6\text{Li} + {}^{12}\text{C}$ scattering angular distributions between 24 and 50 MeV: (a) Nearside/farside contributions (thin lines) and (b) barrier-wave (dashed line)/internal-wave (dash-dotted line) contributions to the OM elastic scattering cross section (thick line) at 30 MeV; (c) and (d) farside (thin line), barrier-wave (dashed line), and internal-wave (dash-dotted line) contributions to the OM elastic scattering cross section (thick line) at 24 and 50 MeV.

More direct evidence for the transparency of the system is provided by the barrier-wave/internal-wave decomposition of the scattering amplitude, which separates cleanly the two interfering components of the amplitude responsible for the Airy structure [14,15]. Although this approach was initially introduced within a semiclassical context [22], it is in most cases possible to avoid the difficult semiclassical calculations and to perform the B/I decomposition using an ordinary OM code [23]. The barrier-wave and internal-wave components of the amplitude have an intuitively very simple meaning: They correspond, respectively, to the part of the incident flux that is reflected at the effective potential barrier and to that which crosses the barrier and reemerges in the elastic channel after reflection at the most internal turning point. When absorption is strong this last component has no chance to survive and

the angular distribution is dominated by the barrier-wave contribution on the whole angular range; the observation of a substantial internal-wave contribution thus also points to the transparency of the system under investigation. We note that in contrast to the N/F decomposition, which can in principle be carried out at any energy, the B/I decomposition is restricted to energies lower than the critical energy where the effective potential pocket disappears at the grazing angular momentum, which as can be seen in Fig. 4 is about 30 MeV in the c.m. for the present system (corresponding to a critical angular momentum of about $12\hbar$).

The B/I decomposition of the 30-MeV ${}^6\text{Li} + {}^{12}\text{C}$ OM angular distribution, obtained using the simplified technique of Ref. [23], is presented in Fig. 3(b). One sees that the forward part of the angular distribution is dominated by the

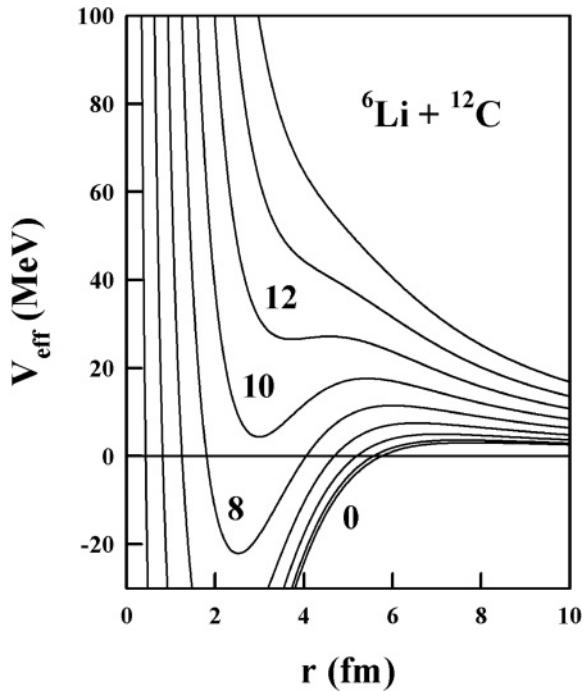


FIG. 4. Effective potential curves calculated for $\ell = 0(2)16$ from the real part of the global potential of the present study with $V_0 = 230$ MeV.

barrier-wave component, whereas the internal-wave component accounts for most of the back-angle region. At intermediate angles, where the two components have a similar magnitude, a strong destructive interference is observed, which accounts for the experimental broad Airy minimum around 100° . On the left of this minimum is a broad plateau, resulting from the interference of the B and I components, which has now become constructive; at still smaller angles the interference turns again to destructive, with the appearance

of the A3 minimum, which is not very conspicuous at this energy. The A3 minimum is, however, observed at 24 MeV around 70° ; it is clearly seen in the farside contribution and is again accounted for by the same B/I destructive interference mechanism as at 30 MeV [Fig. 3(c)]. A similar situation is again encountered at 50 and 54 MeV; this time the Airy minimum observed at 50 MeV near 100° is A1, and on its left side one finds a plateau similar to that observed at 30 MeV and that is due to the same interference mechanism [Fig. 3(d)]. The A2 minimum is also seen at 50 MeV around 45° and is clearly identified in the farside contribution [Fig. 3(d)]. The plateau observed at 50 and 54 MeV is the “exotic feature” correctly identified by Carstoiu *et al.* [24] as a refractive phenomenon; it is in fact not a novel feature, since it is clearly seen, and has the same physical origin, in, for example, $\alpha + {}^{16}\text{O}$ scattering at 39 MeV [39], in several $\alpha + {}^{40}\text{Ca}$ angular distributions below 60 MeV [41], and in ${}^{16}\text{O} + {}^{16}\text{O}$ and ${}^{16}\text{O} + {}^{12}\text{C}$ scattering between 5 and 10 MeV per nucleon [10–15].

To summarize the situation, it is useful to plot the location of the Airy minima of various orders as a function of the incident c.m. energy; this is presented in Fig. 5, together with the results obtained from the global $\alpha + {}^{16}\text{O}$ potential of Ref. [39]. At a given angle the passing of these minima as energy increases produces broad minima in the excitation function measured at this angle. Such a structure was observed by Vineyard *et al.* [29] in the excitation functions measured at 98° and 120° between 20 and 36 MeV. Figure 6 shows that the experimental structure is well reproduced by the present global optical potential; the curves were generated by using parameters linearly interpolated from Table I. The observed minima are essentially due to the passing of the A3 and A2 Airy minima at these angles. The excitation function at 37.2° is also well reproduced by our calculation (Fig. 6), but the broad minimum observed around 27 MeV at this smaller angle is simply due to the passing of a Fraunhofer diffraction minimum (see Fig. 1).

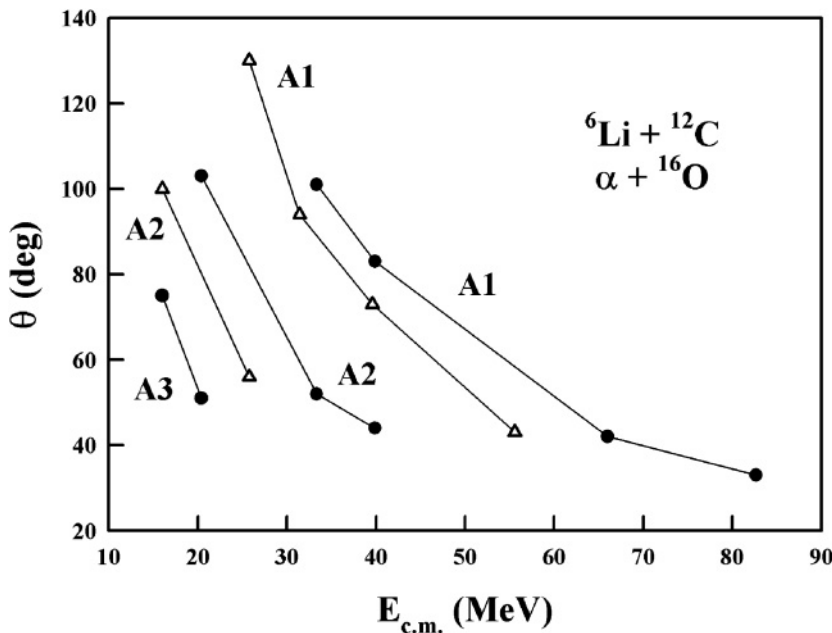


FIG. 5. Evolution with energy of the angular position of the Airy minima of various orders observed in the ${}^6\text{Li} + {}^{12}\text{C}$ (dots) and $\alpha + {}^{16}\text{O}$ (triangles) elastic scattering angular distributions.

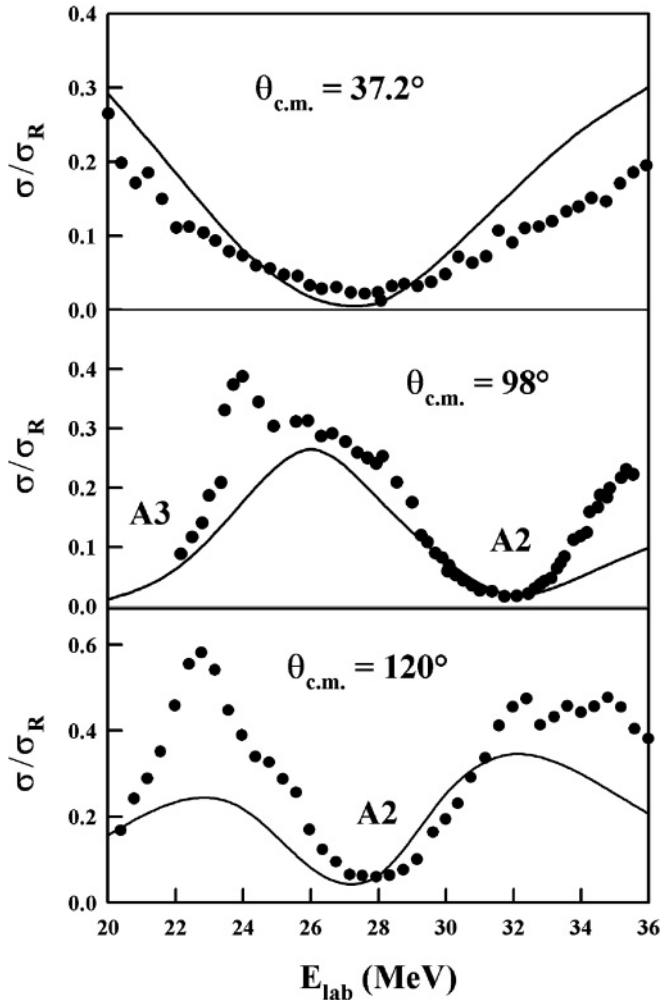


FIG. 6. Comparison of the experimental ${}^6\text{Li} + {}^{12}\text{C}$ excitation functions between 20 and 36 MeV at 37.2° , 98° , and 120° [29] with the predictions of the global optical potential, and identification of several Airy minima contributing to the observed structure.

The surprising transparency displayed by ${}^6\text{Li} + {}^{12}\text{C}$ scattering, which on account of breakup effects could have been expected to be dominated by strong absorption, can also be illustrated by looking at the scattering reflection coefficients. These are presented in Fig. 7 at 13, 30, and 50 MeV, together with their barrier-wave and internal-wave components; whereas the barrier-wave contribution has a characteristic strong absorption profile [42] and is negligible at low ℓ except at the lowest energy, the internal-wave reflection coefficients attain values of the order of 0.1, not very different from those observed in the case of the very transparent $\alpha + {}^{16}\text{O}$ system at comparable energies [39].

It is interesting to inquire whether the transparency observed in elastic scattering data persists in some inelastic channels. Indeed it has recently been shown by the present authors within the frame of the distorted-wave Born approximation (DWBA) that for light-ion and light heavy-ion systems displaying incomplete absorption, a substantial internal-wave component can survive in the backward hemisphere in some

inelastic channels as well, causing a B/I interference pattern similar to that observed in the elastic channel [43].

${}^{12}\text{C}({}^6\text{Li}, {}^6\text{Li}'){}^{12}\text{C}^*$ scattering has been measured at 24 and 30 MeV by Vineyard *et al.* [44] for the excitation of the $J^\pi = 2^+$ (4.44 MeV), 0^+ (7.65 MeV), and 3^- (9.64 MeV) states of ${}^{12}\text{C}$ up to about 170° in the c.m. We investigated the angular distributions corresponding to the excitation of the $J^\pi = 2^+$ rotational state of ${}^{12}\text{C}$ within the frame of a coupled channels (CC) approach; the agreement with the data of the DWBA and CC calculations reported by Vineyard *et al.* [44] for this state is qualitative at best at intermediate and large angles. To avoid “parameter fiddling,” we decided to restrict ourselves to a minimal analysis: Starting from the OM parameters listed in Table I, we simply readjusted the real and imaginary well depths V_0 and W_0 , and adjusted the (real) deformation parameter β_2 to the elastic and inelastic angular distributions at 30 MeV, using the coupled channel code ECIS [45]. Good agreement in the two channels was obtained for parameter values $V_0 = 210.3$ MeV, $W_0 = 12.7$ MeV, and $\beta_2 = -0.55$. The sign of the real and imaginary potential changes is compatible with the polarization potentials arising from nuclear inelastic scattering—which are predominantly attractive and absorptive, respectively [46].

The agreement with the elastic scattering data is comparable to that reported in Figs. 1 and 3 and is not illustrated here; a comparison of our results with the inelastic data is presented in the lower part of Fig. 8. The deformation parameter extracted is compatible with the values quoted in the literature [47]. Although phasing with experiment is not perfect at large angles, the agreement obtained is very satisfactory, especially if one takes into account the fact that ${}^{12}\text{C}$ is strongly deformed and that a more precise calculation should take into account its hexadecapole deformation; in addition, explicit coupling to the 0^+ (7.65 MeV) and 3^- (9.64 MeV) states should also be considered.

At 24 MeV, we simply used the same deformation parameter and the same potential as at 30 MeV, except for the imaginary potential depth, which was tuned to the smaller value $W_0 = 10.5$ MeV. As can be seen in the upper part of Fig. 8, an excellent agreement is obtained over the whole angular range. In particular, the change of slope observed in the experimental data around 80° is quantitatively well reproduced by the calculation. We also note that the theoretical curves display some oscillations in the backward hemisphere, whereas the data are practically structureless; a damping of the oscillations in the CC curve is, however, expected to appear when additional channels are explicitly coupled to the entrance channel.

Finally, we subjected the inelastic scattering amplitude to a B/I decomposition, using the same technique as that introduced in Ref. [43] within the frame of the DWBA. Thus we added a strong, narrow absorptive term in the calculation, located at the minimum of the real effective potential curve at the grazing angular momentum, to cancel the internal-wave contribution to the scattering. In a second step the barrier-wave inelastic amplitude obtained in this way was subtracted from the full inelastic scattering amplitude, which provided us with the internal-wave contribution. To perform this decomposition, use was made in the ECIS calculation of

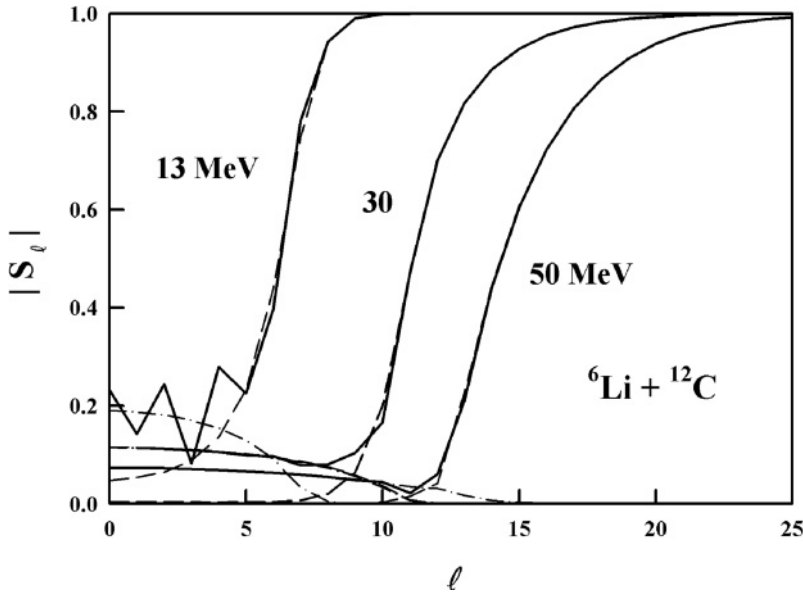


FIG. 7. Decomposition of the modulus of the ${}^6\text{Li} + {}^{12}\text{C}$ optical model S matrix (thick lines) into its barrier-wave (dashed lines) and internal-wave (dash-dotted lines) components at 13, 30, and 50 MeV.

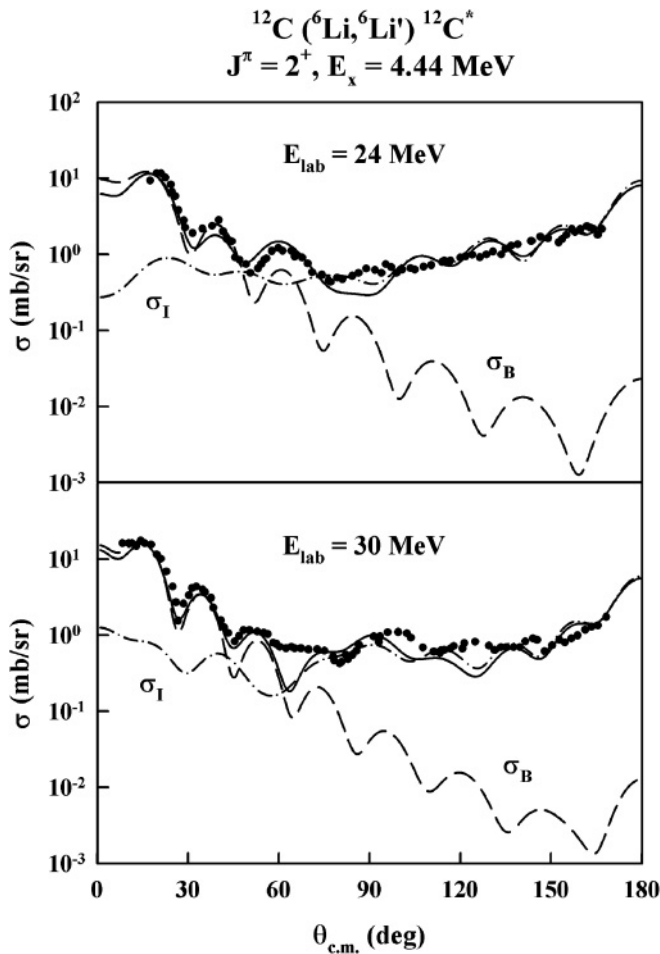


FIG. 8. Comparison of the experimental ${}^{12}\text{C}({}^6\text{Li}, {}^6\text{Li}'){}^{12}\text{C}^*$ ($J^\pi = 2^+$, $E_x = 4.44$ MeV) inelastic scattering data of Vineyard *et al.* [44] at 24 and 30 MeV with the results of coupled channel calculations (full line); the barrier-wave and internal-wave contributions to the inelastic angular distributions are presented as dashed lines and dash-dotted lines, respectively.

an extra Woods-Saxon derivative imaginary surface potential; in conventional notation, the parameters of the latter are $W_s = 50$ MeV, $R_s = 3$ fm, and $a_s = 0.5$ fm. The B/I contributions to inelastic scattering at 24 and 30 MeV are presented in Fig. 8. It is seen that the backward inelastic angular distributions are, as is the case in the elastic channel, completely dominated by the internal contribution. In particular, the continuous rise observed at 24 MeV beyond 80° is entirely due to the internal component and is thus associated with deeply penetrating trajectories; the surprising transparency observed in ${}^6\text{Li} + {}^{12}\text{C}$ scattering is thus not restricted to the elastic channel.

IV. REFRACTIVE EFFECTS IN NEIGHBORING SYSTEMS

Airy minima are clearly seen in the elastic angular distributions for neighboring systems such as ${}^6\text{Li} + {}^{16}\text{O}$ or ${}^7\text{Li} + {}^{12}\text{C}$; this shows that the puzzling transparency observed in ${}^6\text{Li} + {}^{12}\text{C}$ scattering is not restricted to this system, but seems to be characteristic of this projectile/target mass range. Unfortunately for these systems there exist no systematic measurements on the full angular and energy ranges comparable to those available for ${}^6\text{Li} + {}^{12}\text{C}$, and it is thus difficult to identify unambiguously the order of the observed Airy minima.

The ${}^6\text{Li} + {}^{16}\text{O}$ angular distribution at 29.8 MeV incident energy [20] is remarkably similar to the ${}^6\text{Li} + {}^{12}\text{C}$ 30-MeV angular distribution; it turned out to be easily reproduced within the OM, using potential parameters close to those used for ${}^6\text{Li} + {}^{12}\text{C}$ at 30 MeV. The diffuseness of the real part of the potential was fixed to the value obtained for the ${}^6\text{Li} + {}^{12}\text{C}$ case, that is, $a_R = 0.7$ fm; the other parameters derived from the fit assume the values $V_0 = 316.2$ MeV, $R_R = 3.319$ fm, $W_0 = 11.5$ MeV, $R_I = 5.822$ fm, and $a_I = 0.613$ fm, to which correspond volume integrals per nucleon pair $J_V/96 = 420$ MeV fm³ and $J_W/96 = 70.7$ MeV fm³. The fit corresponding to these parameters is presented in Fig. 9, together with the barrier-wave, internal-wave, and farside contributions

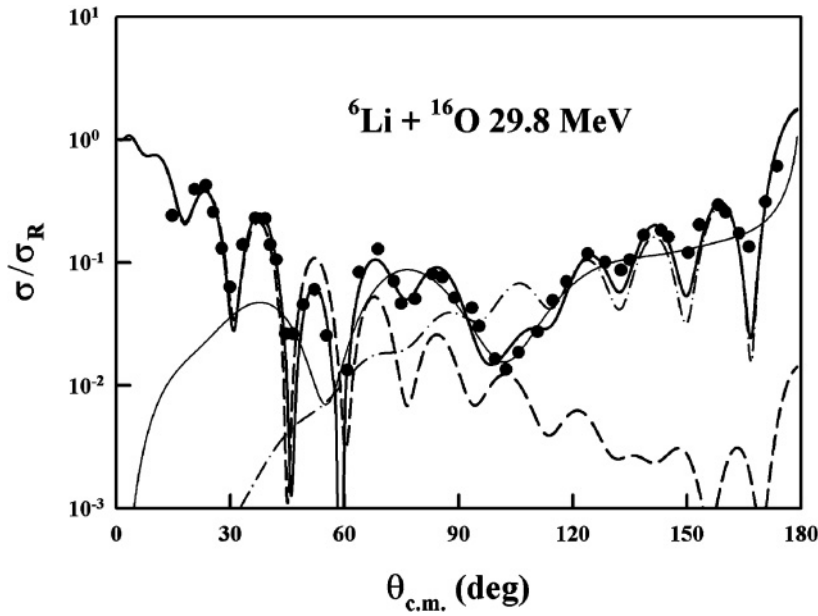


FIG. 9. Farside (thin line), barrier-wave (dashed line), and internal-wave (dash-dotted line) contributions to the ${}^6\text{Li} + {}^{16}\text{O}$ OM cross section (thick line) at 29.8 MeV, together with the experimental data of Ref. [20].

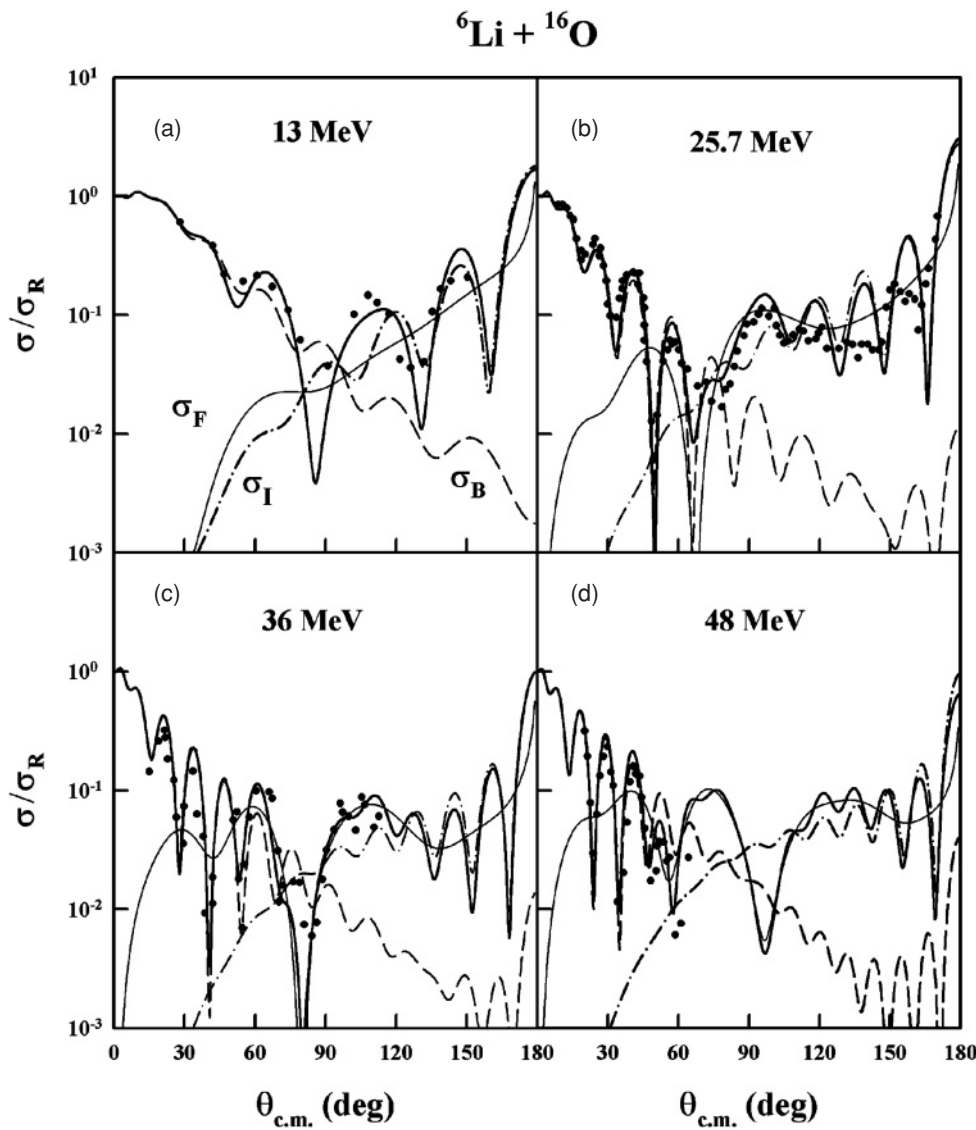


FIG. 10. Comparison of the predictions (see text) of the 29.8-MeV ${}^6\text{Li} + {}^{16}\text{O}$ OM potential at 13, 25.7, 36, and 48 MeV (thick line) with the experimental data of Refs. [28,29,48,49], and farside (thin line), barrier-wave (dashed line), and internal-wave (dash-dotted line) contributions to the OM cross section.

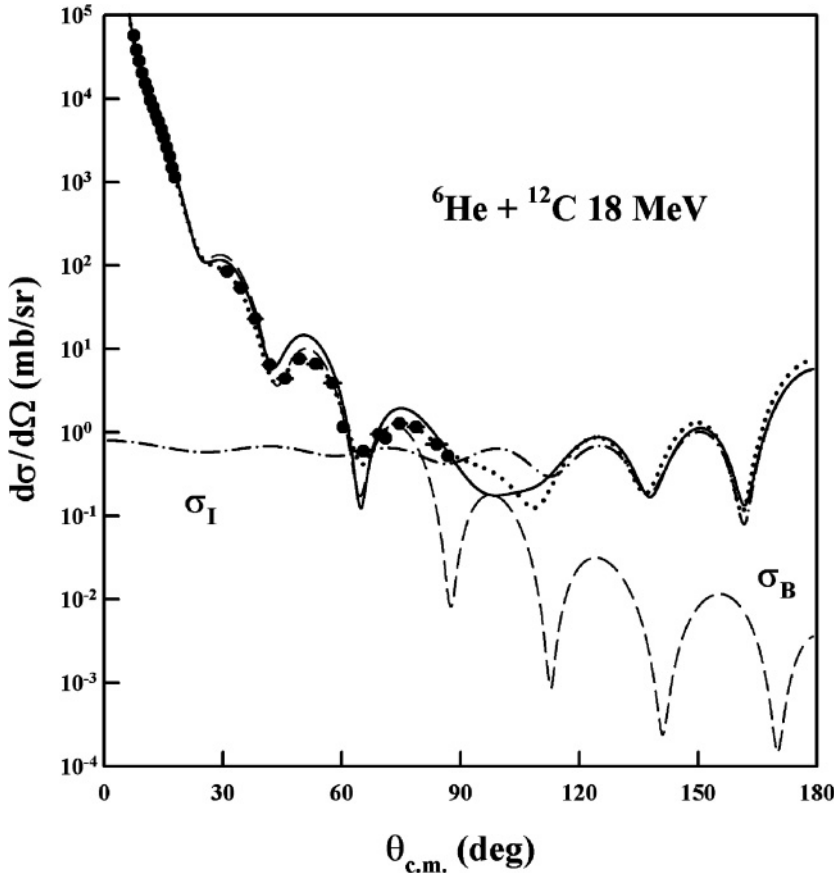


FIG. 11. Comparison with the 18-MeV ${}^6\text{He} + {}^{12}\text{C}$ elastic scattering data of Milin *et al.* [1] of the OM predictions of the potential OM1 of Trcka *et al.* [25] (thick line), together with its barrier-wave (dashed line) and internal-wave (dash-dotted line) components, and of the Woods-Saxon squared potential of the present study (dotted line).

to the scattering. The comments concerning the transparency of the ${}^6\text{Li} + {}^{12}\text{C}$ system can evidently be repeated here.

As few experimental data are available for this system we tested the predictive power of this potential by simply rescaling W_0 at each energy. This proved to provide a good overall representation of the data at 13 [28], 25.7 [29], 36 [48], and 48 MeV [49] (Fig. 10), using the values $W_0 = 7, 10, 13.5,$ and 16 MeV, respectively, at these four energies. In particular the potential predicts correctly the shift of the Airy minimum from about 100° to 80° when energy increases from 29.8 to 36 MeV; the present potential interprets this minimum as A2. The calculation predicts a further shift of this minimum to about 60° at 48 MeV, and the appearance of another minimum at about 100° at this energy, which the potential used here interprets as A1. Likewise the minimum seen around 50° at 29.8 MeV (A3) is correctly predicted to shift to 70° when energy decreases to 25.7 MeV (Fig. 10). To confirm these attributions, additional measurements of the ${}^6\text{Li} + {}^{16}\text{O}$ angular distributions, extending over a sufficient angular range, are needed at higher energy; continuity arguments with the description of the ${}^6\text{Li} + {}^{12}\text{C}$ system, however, make us confident that the present attributions are the correct ones.

V. POSSIBLE REFRACTIVE EFFECTS IN ${}^{12}\text{C}({}^6\text{He}, {}^6\text{He})$ SCATTERING

The remarkable transparency displayed by the ${}^6\text{Li} + {}^{12}\text{C}$ and ${}^6\text{Li} + {}^{16}\text{O}$ systems, despite the importance of breakup effects, opens the possibility of observing a similar phenomenon

in collisions involving weakly bound, radioactive projectiles, such as the recently investigated ${}^6\text{He} + {}^{12}\text{C}$ collision. We thus conclude this study by returning to the new data obtained recently by Milin *et al.* [1] for ${}^{12}\text{C}({}^6\text{He}, {}^6\text{He})$ scattering at 18 MeV incident energy. These data, extending to about 85° in the center of mass, have been correctly fit by Milin *et al.* [1] by using one of the Woods-Saxon potentials (OM1) used by Trcka *et al.* [25] to describe ${}^6\text{Li} + {}^{12}\text{C}$ scattering at 20 MeV (Fig. 11). In Fig. 11 we have also plotted the barrier-wave and internal-wave contributions corresponding to this potential. One sees that in the range spanned by the experimental data, scattering is completely dominated by the barrier-wave component, except for the very last data points; the effect of the internal-wave contribution reveals itself only by weak interference effects with the barrier component. At larger angles the converse situation is observed: The internal-wave component predicted by the OM1 potential dominates the large-angle data, and at intermediate angles ($\theta_{\text{c.m.}} \simeq 100^\circ$) a well-marked, broad interference minimum is observed.

We also obtained an excellent OM fit to these data by using a Woods-Saxon squared potential with a geometry for the real part similar to that used in the present ${}^{12}\text{C}({}^6\text{Li}, {}^6\text{Li})$ analysis. The extracted parameters are $V_0 = 256.5$ MeV, $R_R = 3.079$ fm, $a_R = 0.645$ fm, $W_0 = 17.0$ MeV, $R_I = 4.0$ fm, and $a_I = 1.20$ fm; the real volume integral per nucleon pair, $J_V/72 = 361.3$ MeV fm³, is comparable to that obtained for ${}^6\text{Li} + {}^{12}\text{C}$. It is interesting to point out that in the angular region where no data are available the predictions of that potential are remarkably similar to those obtained from the Trcka potential

(Fig. 11), although no constraint was introduced in the fit for that purpose; the B/I contents of the scattering amplitude is nearly identical for the two potentials. One can tentatively interpret this result by assuming that the last data points, and perhaps also the exact amplitude of the experimental oscillations, contain sufficient information about the (small) internal-wave contribution to constrain the potential fit toward this particular solution. This point can, however, only be settled by carrying out additional measurements extending somewhat beyond the angular range of the presently available data; if confirmed this result would eventually point to a transparency of $^{12}\text{C}(^6\text{He},^6\text{He})$ scattering comparable to that seen in $^6\text{Li} + ^{12}\text{C}$. We consider that the observation of the broad interference minimum predicted around 100° would provide strong evidence for this transparency.

VI. SUMMARY AND CONCLUSIONS

The central result of the present paper is to have shown that the remarkable transparency displayed at low energy by several scattering systems involving strongly bound (light-ion or light heavy-ion) projectiles and targets, such as $\alpha + ^{16}\text{O}$ and $\alpha + ^{40}\text{Ca}$, or $^{16}\text{O} + ^{16}\text{O}$ and $^{16}\text{O} + ^{12}\text{C}$, clearly persists in systems such as $^6\text{Li} + ^{12}\text{C}$ or $^6\text{Li} + ^{16}\text{O}$: Despite breakup effects, fragile projectiles like ^6Li thus have a significant chance to survive a close encounter with the target. Our analysis suggests that this surprising transparency could even be observed in more exotic systems involving weakly bound, radioactive projectiles such as ^6He ; however, additional measurements are needed to settle the issue.

On the theoretical side we think that calculations investigating the importance of breakup effects in these fragile systems are urgently needed at low energy to shed some light on this unexpected transparency: Indeed, most of the existing studies have been restricted to energies greater than or equal to about 10 MeV per nucleon. It is also important to point out that some of these calculations, which connect the reduction of the real part of the folding potential with a strong positive (repulsive) real component of the dynamical polarization potential associated with ^6Li breakup, obtain a negligible imaginary component of the DPP in the peripheral region. However, these calculations assume a strong absorption regime for the scattering, which is thus supposed—in contradiction with the present findings—to be insensitive to the potential at small distances, and accordingly the DPP was only estimated for angular momenta larger than the grazing angular momentum; we think it is important to extend these calculations to the full radial range to test the general compatibility of the underlying models with the experimental evidence.

ACKNOWLEDGMENTS

The authors are very grateful to Carmen Angulo for her help and to Matko Milin for sending us his $^{12}\text{C}(^6\text{He},^6\text{He})$ data. S.O. thanks Dao T. Khoa for valuable discussions on rainbow scattering and for the warm hospitality extended to him during his stay in Hanoi (winter 2004) supported by JSPS. S.O. has been supported by a Grant-in-Aid for Scientific Research of the Japan Society for Promotion of Science (No. 16540265) and the Yukawa Institute for Theoretical Physics.

-
- [1] M. Milin, S. Cherubini, T. Davinson, A. Di Pietro, P. Figuera, D. Miljanić, A. Musumarra, A. Ninane, A. N. Ostrowski, M. G. Pellegriti, A. C. Shotter, N. Soić, C. Spitaleri, and M. Zadro, *Nucl. Phys.* **A730**, 285 (2004).
- [2] G. R. Satchler and W. G. Love, *Phys. Rep.* **55**, 183 (1979).
- [3] Y. Hirabayashi and Y. Sakuragi, *Phys. Lett.* **B258**, 11 (1991).
- [4] Y. Hirabayashi, Y. Sakuragi, and M. Tanifuji, *Phys. Lett.* **B318**, 32 (1993).
- [5] Y. Sakuragi, *Phys. Rev. C* **35**, 2161 (1987).
- [6] Y. Sakuragi, M. Kamimura, and K. Katori, *Phys. Lett.* **B205**, 204 (1988).
- [7] Y. Sakuragi, M. Yahiro, and M. Kamimura, *Prog. Theor. Phys. Suppl.* **89**, 136 (1986); Y. Hirabayashi, *Phys. Rev. C* **44**, 1581 (1991); Y. Sakuragi, M. Ito, Y. Hirabayashi, and C. Samanta, *Prog. Theor. Phys.* **98**, 521 (1997); C. Samanta, Y. Sakuragi, M. Ito, and M. Fujiwara, *J. Phys. G* **23**, 1697 (1997).
- [8] F. Michel, S. Ohkubo, and G. Reidemeister, *Prog. Theor. Phys. Suppl.* **132**, 7 (1998) and references therein.
- [9] M. E. Brandan and G. R. Satchler, *Phys. Rep.* **285**, 143 (1997) and references therein.
- [10] M. P. Nicoli, F. Haas, R. M. Freeman, N. Aissaoui, C. Beck, A. Elanique, R. Nouicer, A. Morsad, S. Szilner, Z. Basrak, M. E. Brandan, and G. R. Satchler, *Phys. Rev. C* **60**, 064608 (1999).
- [11] Dao T. Khoa, W. von Oertzen, H. G. Bohlen, and F. Nuoffer, *Nucl. Phys.* **A672**, 387 (2000).
- [12] M. P. Nicoli, F. Haas, R. M. Freeman, S. Szilner, Z. Basrak, A. Morsad, G. R. Satchler, and M. E. Brandan, *Phys. Rev. C* **61**, 034609 (2000).
- [13] A. A. Ogloblin, Yu. A. Glukhov, V. Trzaska, A. S. Dem'yanova, S. A. Goncharov, R. Julin, S. V. Klebnikov, M. Mutterer, M. V. Rozhkov, V. P. Rudakov, G. P. Tiorin, D. T. Khoa, and G. R. Satchler, *Phys. Rev. C* **62**, 044601 (2000).
- [14] F. Michel, F. Brau, G. Reidemeister, and S. Ohkubo, *Phys. Rev. Lett.* **85**, 1823 (2000).
- [15] F. Michel, G. Reidemeister, and S. Ohkubo, *Phys. Rev. C* **63**, 034620 (2001).
- [16] M. S. Hussein and K. W. McVoy, *Prog. Part. Nucl. Phys.* **12**, 103 (1984).
- [17] K. W. McVoy, H. M. Khalil, M. S. Shalaby, and G. R. Satchler, *Nucl. Phys.* **A455**, 118 (1986).
- [18] K. W. McVoy and M. E. Brandan, *Nucl. Phys.* **A542**, 295 (1992).
- [19] M. E. Brandan, M. S. Hussein, K. W. McVoy, and G. R. Satchler, *Comments Nucl. Part. Phys.* **22**, 77 (1996).
- [20] V. I. Chuev, V. V. Davidov, B. G. Novatskii, A. A. Ogloblin, S. B. Sakuta, and D. N. Stepanov, *J. Phys. (Paris) Suppl.* **C 6**, 161 (1971).
- [21] G. Bassani, N. Saunier, B. M. Traore, J. Raynal, A. Foti, and G. Pappalardo, *Nucl. Phys.* **A189**, 353 (1972).
- [22] D. M. Brink and N. Takigawa, *Nucl. Phys.* **A279**, 159 (1977); D. M. Brink, *Semi-classical Methods for Nucleus-Nucleus*

- Scattering* (Cambridge University Press, Cambridge, U.K., 1985).
- [23] J. Albiński and F. Michel, *Phys. Rev. C* **25**, 213 (1982).
- [24] F. Carstoiu, L. Trache, R. E. Tribble, and C. A. Gagliardi, *Phys. Rev. C* **70**, 054610 (2004).
- [25] D. E. Trcka, A. D. Frawley, K. W. Kemper, D. Robson, J. D. Fox, and E. G. Myers, *Phys. Rev. C* **41**, 2134 (1990).
- [26] R. C. Fuller, *Phys. Rev. C* **12**, 1561 (1975).
- [27] P. K. Bindal, K. Nagatani, M. J. Schneider, and P. D. Bond, *Phys. Rev. C* **9**, 2154 (1974).
- [28] J. E. Poling, E. Norbeck, and R. R. Carlson, *Phys. Rev. C* **13**, 648 (1976).
- [29] M. F. Vineyard, J. Cook, K. W. Kemper, and M. N. Stephens, *Phys. Rev. C* **30**, 916 (1984).
- [30] H. G. Bingham, M. L. Halbert, D. C. Hensley, E. Newman, K. W. Kemper, and L. A. Charlton, *Phys. Rev. C* **11**, 1913 (1975).
- [31] P. Schwandt, W. W. Jakobs, M. D. Kaitchuck, P. P. Singh, W. D. Ploughe, F. D. Becchetti, and J. Jänecke, *Phys. Rev. C* **24**, 1522 (1981).
- [32] K. Katori, T. Shimoda, T. Fukuda, S. Shimoura, A. Sakaguchi, M. Tanaka, T. Yamagata, N. Takahashi, H. Ogata, M. Kamimura, and Y. Sakuragi, *Nucl. Phys.* **A480**, 323 (1988).
- [33] J. Cook, H. J. Gils, H. Rebel, Z. Majka, and H. Klewe-Nebenius, *Nucl. Phys.* **A388**, 173 (1982); Report KfK 3233, Kernforschungszentrum Karlsruhe, 1981 (unpublished).
- [34] A. Nadasen, M. McMaster, G. Gunderson, A. Judd, S. Villanueva, P. Schwandt, J. S. Winfield, J. van der Plicht, R. E. Warner, F. D. Becchetti, and J. W. Jänecke, *Phys. Rev. C* **37**, 132 (1988).
- [35] A. Nadasen, T. Stevens, J. Farhat, J. Brusoe, P. Schwandt, J. S. Winfield, G. Yoo, N. Anantaraman, F. D. Becchetti, J. Brown, B. Hotz, J. W. Jänecke, D. Roberts, and R. E. Warner, *Phys. Rev. C* **47**, 674 (1993).
- [36] N. A. El-Nohy, F. A. El-Akkad, A. M. Abdel-Monem, and O. S. Abdel-Fattah, *Int. J. Mod. Phys. E* **11**, 437 (2002).
- [37] D. T. Khoa, G. R. Satchler, and W. von Oertzen, *Phys. Rev. C* **51**, 2069 (1995).
- [38] S. Ohkubo, Y. Kondō, and S. Nagata, *Prog. Theor. Phys.* **57**, 82 (1977).
- [39] F. Michel, J. Albiński, P. Belery, Th. Delbar, Gh. Grégoire, B. Tasiaux, and G. Reidemeister, *Phys. Rev. C* **28**, 1904 (1983).
- [40] F. Michel, G. Reidemeister, and S. Ohkubo, *Phys. Rev. Lett.* **89**, 152701 (2002).
- [41] Th. Delbar, Gh. Grégoire, G. Paic, R. Ceuleneer, F. Michel, R. Vanderpoorten, A. Budzanowski, H. Dabrowski, L. Freindl, K. Grotowski, S. Micek, R. Płaneta, A. Strzalkowski, and K. A. Eberhard, *Phys. Rev. C* **18**, 1237 (1978).
- [42] W. E. Frahn, *Diffraction Processes in Nuclear Physics* (Clarendon Press, Oxford, U.K., 1985).
- [43] F. Michel and S. Ohkubo, *Nucl. Phys.* **A738**, 231 (2004); *Phys. Rev. C* **70**, 044609 (2004).
- [44] M. F. Vineyard, J. Cook, and K. W. Kemper, *Phys. Rev. C* **31**, 879 (1985).
- [45] J. Raynal, in *Computing as a language of Physics*, ICTP International Seminar Course, Trieste, Italy, Aug. 2–20, 1971 (IAEA, Vienna, 1972), p. 281.
- [46] Z. El-Itaoui, P. J. Ellis, and B. A. Mughrabi, *Nucl. Phys.* **A441**, 511 (1985).
- [47] M. Yasue, T. Tanabe, F. Soga, J. Kokame, F. Shinokoshi, J. Kasagi, Y. Toba, Y. Kadota, T. Ohsawa, and K. Furuno, *Nucl. Phys.* **A394**, 29 (1983).
- [48] P. Schumacher, N. Ueta, H. H. Duhm, K.-I. Kubo, and J. Klages, *Nucl. Phys.* **A212**, 573 (1973).
- [49] J. Cook, L. C. Dennis, K. W. Kemper, T. R. Ophel, A. F. Zeller, C. F. Maguire, and Z. Kui, *Nucl. Phys.* **A415**, 114 (1984).